ACS Photonics

Article

Cite This: ACS Photonics XXXX, XXX, XXX−XXX

pubs.acs.org/journal/apchd5

Accurate Background Subtraction in STED Nanoscopy by Polarization Switching

Jong-Chan Lee,[†,‡] Ye Ma,[§] Kyu Young Han,[∥] and Taekjip Ha*[,‡,§,⊥]

[†]Department of New Biology, DGIST, Daegu, Republic of Korea

[‡]Department of Biophysics and Biophysical Chemistry, Johns Hopkins University, Baltimore, Maryland, United States

[§]Department of Biomedical Engineering, Johns Hopkins University, Baltimore, Maryland, United States

[∥]CREOL, The College of Optics and Photonics, University of Central Florida, Orlando, Florida, United States

[⊥]Howard Hughes Medical Institute, Baltimore, Maryland, United States

Supporting Information

ABSTRACT: STED nanoscopy helped usher in resolution revolution of optical microscopy and has been widely used to study subcellular structures and dynamics. To achieve optical resolution beyond the diffraction limit, STED nanoscopy employs 10^4−10^5 times more intense light compared to conventional imaging methods, giving rise to additional background that can be detrimental to imaging and quantification of dense samples. Here, we report a simple and easy-to-implement method to suppress background noise by polarization switching (psSTED). STED imaging requires a well-defined polarization state of a STED laser (typically left-circular polarization). By switching to right-circular polarization, the spatial profile of the STED laser changes to fill up the center of the donut-shaped beam, enabling an accurate background recording. Through a straightforward subtraction of the recorded background from the regular STED image, we achieved background-subtracted STED imaging. With simulation and experiment, we demonstrate that psSTED outperforms other background subtraction methods.

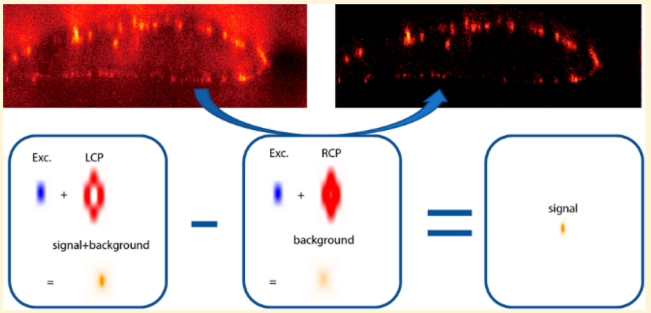

KEYWORDS: *super-resolution microscopy, STED nanoscopy, background noise, background suppression, optical resolution*

Enabling imaging with a resolution beyond the optical diffraction limit, super-resolution microscopy, or optical nanoscopy has revolutionized our ability to probe biological structures and dynamics that could not be seen with conventional optical imaging tools.[1−3] In STimulated Emission Depletion (STED) nanoscopy,[3−5] a laser beam, called the STED beam, is wavefront modulated and shaped into a hollow spot to deplete the off-the-center fluorescence to reveal details beyond the diffraction limit. Ideally, the STED beam should only function to de-excite the molecules at the periphery of the excitation spot. However, because it is typically 4−5 orders of magnitude more intense than the fluorescence excitation beam, it can directly excite the fluorescent molecules.[6] Furthermore, the relatively low intensity at the periphery of the STED spot can incompletely deplete the fluorescence signal, leading to off-center fluorescence leakage. Both direct excitation and incomplete depletion contribute to a low-spatial-frequency fluorescence background, which can mask the high spatial frequency super-resolved fluorescence signal.

Background suppression is even more critical in 3D STED.[7−9] The out-of-focus background and low-spatial-frequency background in 3D STED are so large as to obscure finer details that STED imaging should reveal. Additional photon flux from the Z-STED beam, introduced for axial confinement results in higher direct excitation. Fluorescence signal itself is reduced because of a residual STED beam at the center of the spot. The decreased signal-to-background ratio (SBR) by both decreased signal and increased background calls for an approach to suppress the background accurately in 3D STED.

There have been several reports addressing this background issue.[10−18] To correct for the background from direct excitation, a general category of methods we call here STED-only subtraction (sub-STED) have been used. In sub-STED, a background image is acquired with only the STED beam on and is subtracted from the regular STED image.[11,12] To suppress the background coming from incomplete depletion, a method called stimulated emission double depletion (STEDD) has been introduced, where a second STED pulse of Gaussian beam profile is applied to estimate the background.[13,14] However, there is ambiguity in choosing the intensity of the second STED beam and the subtraction factor, which potentially raises the risk of oversubtraction. Gating the fluorescence detection time has also been used for background suppression.[15−18]

Received: April 9, 2019
Published: June 13, 2019

DOI: 10.1021/acsphotonics.9b00537
ACS Photonics XXXX, XXX, XXX−XXX

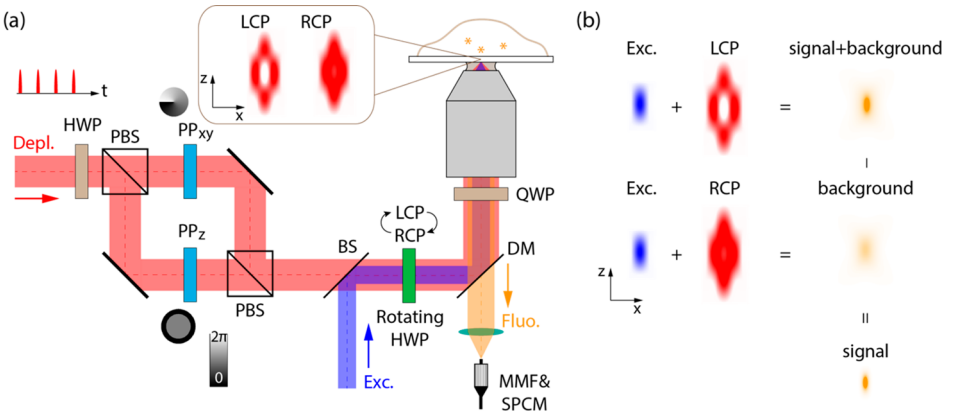

Figure 1. Principle of psSTED. (a) Schematic of the experiment. Depletion laser (Depl.) is launched and split at the polarizing beam splitter (PBS), where the split ratio is tuned by a half-wave plate (HWP). Two phase plates, PP_{xy} and PP_z, generate the XY- and Z-STED profiles at the objective lens focus, respectively. The depletion laser is then combined at another PBS and combined with an excitation beam at the 70:30 beam splitter (BS). HWP and quarter-wave plate (QWP) are used to precisely align the polarization to left-circular polarization (LCP). Polarization switching takes place at a HWP shown in green, such that LCP is modulated to right-circular polarization (RCP) by a motorized rotation stage. As shown in the inset, the 3D STED spatial profile of RCP has a filled center compared with that of LCP. STED and the excitation laser are reflected at the dichroic mirror (DM) and enter the objective lens to illuminate certain focal volumes at the specimen. The fluorescence from the specimen is spectrally filtered by DM, and additional filters (not shown in figure) are used for detection. Finally, the fluorescence is focused to the tip of a multimode fiber (MMF), which acts as a pinhole of size 62.5 μm and delivers photons to a single-photon counting module (SPCM). For a detailed schematic of the experiment, see Supporting Information. (b) Working principle of the method. When LCP is used for the depletion laser, the image records signal and background-like conventional STED. When polarization is changed to RCP, the signal at the center is also depleted, and the image records the background noise. By subtracting the two images, background-subtracted psSTED is achieved.

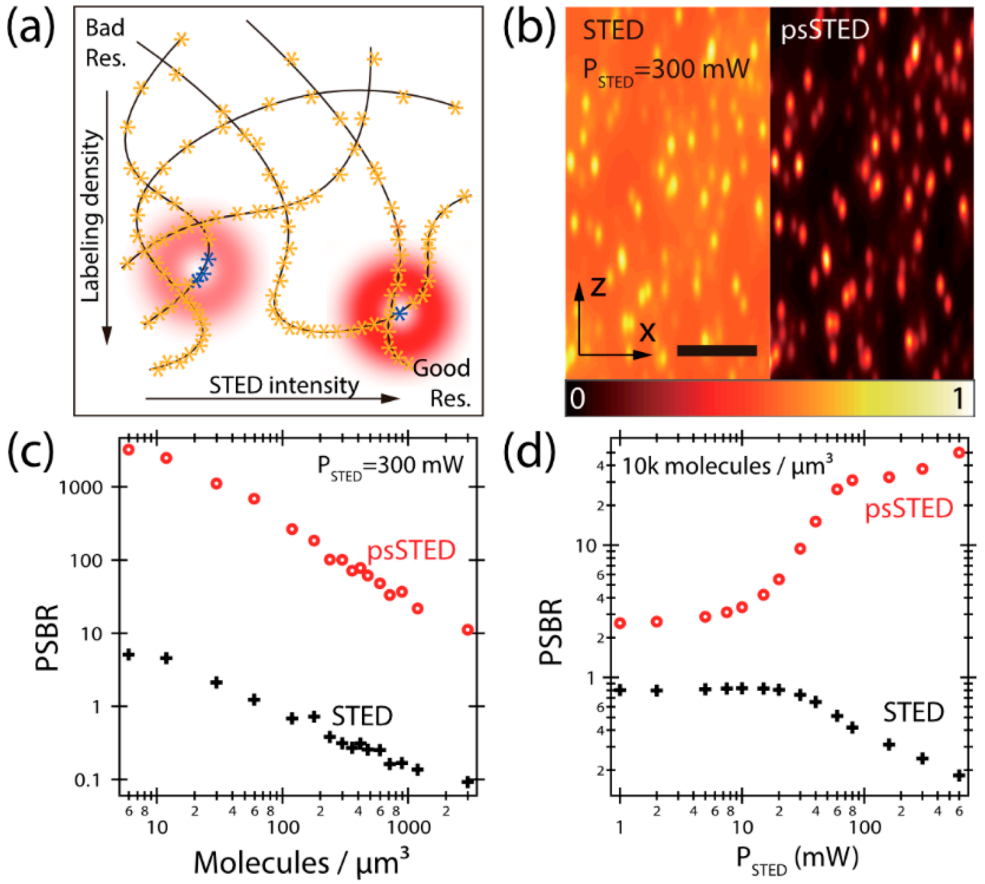

Figure 2. Background noise problem in STED and significant background reduction by psSTED. (a) Achieving higher resolution requires both strong STED intensity as well as high fluorescence labeling density. (b) An example of 10000 simulated randomly located fluorescent molecules, both seen with conventional STED and psSTED methods. Randomly located fluorescent molecules in 3D space are simulated to investigate the effect of labeling density (c) and STED power (d) to peak signal-to-background ratio (PSBR) in STED imaging.

DOI: 10.1021/acsphotonics.9b00537
ACS Photonics XXXX, XXX, XXX−XXX

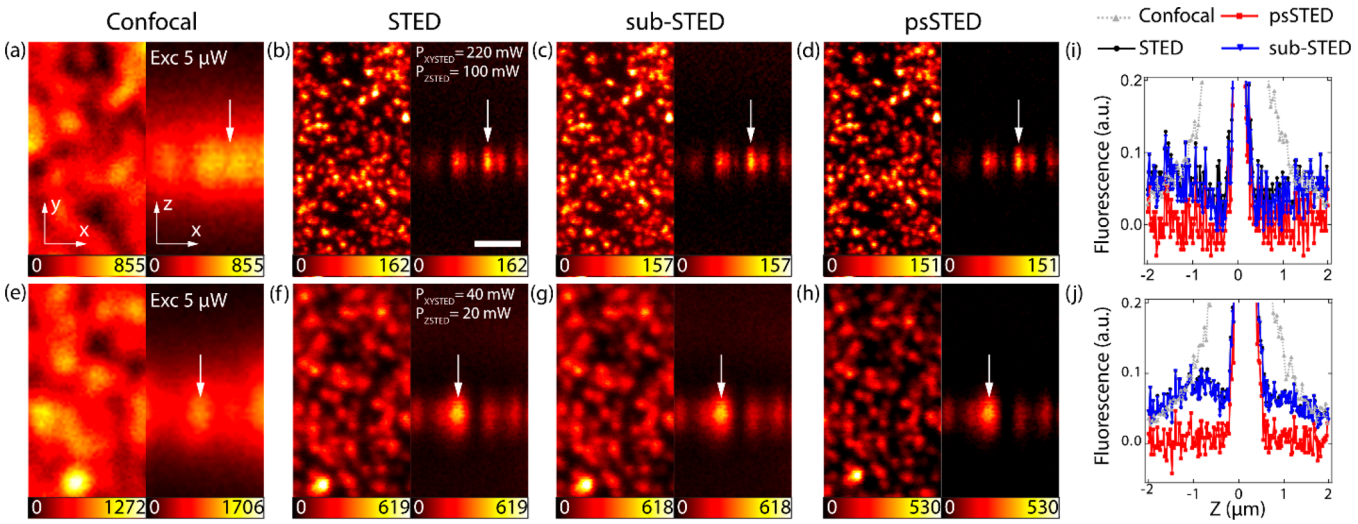

Figure 3. Experimental images of fluorescent beads. The beads are localized in XY plane of the imaging volume. Two STED power conditions are used: high power (XY STED: 220 mW, Z STED: 100 mW, (a)−(d)) and low power (XY STED: 40 mW, Z STED: 20 mW, (e)−(h): (a, e) confocal, (b, f) conventional STED, (c, g) sub-STED, and (d, h) 2D psSTED images. XY and XZ cross-section of the bead sample images are shown in all conditions. (i) Cross-section of a bead along the *z* axis (white arrow) in images (a)−(d). (j) Cross-section along *z* (white arrow) in images (e)−(h). The sampling steps: 10 nm in XY, 20 nm in Z. Pixel dwell time: 400 μs. Scale bar: 500 nm.

We herein propose polarization switching STED (psSTED) that can accurately suppress the low spatial frequency background appearing in STED images. In psSTED, we switch the STED beam polarization between two different circularly polarized states to record a regular STED image and a background image sequentially. A straightforward, unambiguous subtraction process between these two images provides us with a background-subtracted super-resolved image. With simulations and experimentations, we demonstrate psSTED for both the high STED power regime where the background due to direct excitation by STED beam is strong, and the low STED power regime where the background is mostly due to incomplete depletion. Comparison of the background suppression performance of psSTED with the sub-STED,[11] time-gated detection[15] (g-STED), and STEDD[13,14] highlights its capability of accurate background suppression with a simple hardware implementation.

RESULTS

Working Principle of psSTED. psSTED makes use of the fact that the STED spot generated by phase modulation is also polarization-dependent[19] (Figure 1 and Supporting Information, Figure S1). Suppose that a counterclockwise vortex phase plate is used for generating the XY-STED spot. Only when the STED beam is left-handed circularly polarized (LCP) can we get a donut spot with a theoretically predicted zero-intensity center. By comparison, for a right-handed circularly polarized (RCP) beam, the longitudinal component of the electric field constructively interferes at the center and fills the hollow center of the STED donut, rather than destructively interfering, as in a LCP beam (Supporting Information, Figure S2). Combined with the unaffected Z-STED spot, the RCP STED beam will be focused into a 3D pattern that has almost the same exterior contour as the regular 3D STED hollow profile, while the center is filled. This RCP STED spot depletes the fluorescence signal at the center, and only the background fluorescence, due to the incomplete depletion and the direct excitation by the STED beam, is detected (Figure 1). The image recorded when both the fluorescence excitation and RCP STED beams are turned on is an accurate estimation of the background and can be subtracted from the regular STED image (obtained using the LCP STED beam), resulting in a background-subtracted super-resolved image (Figures 1b, Figure 2, and Figure S3).

Theory and Simulation of psSTED. To predict the performance of psSTED in background suppression, we conducted several simulations assuming a three-level energy system for fluorophores (see Supplementary Text for details). A set of differential equations is used to describe the temporal evolution of each state's population. After solving the equations numerically, we can calculate the detectable fluorescence. Images with different STED beam powers and polarizations can therefore be simulated with a prescribed intensity distribution of STED beam in space. For estimating the background arising from excitation by the STED beam, we included both the re-excitation (after STED-induced de-excitation) and the direct excitation process by the STED beam (Supporting Information, Figure S4). Under our experimental conditions where we employ a 100 ps excitation pulse and a 300 ps STED pulse, the effect caused by STED re-excitation is small compared with the direct excitation by the STED beam. Simulated STED images of a single layer of beads show different background profiles between high STED power (XY-STED: 200 mW; Z-STED: 100 mW) and low STED power (XY-STED: 40 mW; Z-STED: 20 mW, Supporting Information, Figures S5 and S6) because direct excitation-induced background increases with increasing STED power, while background due to incomplete depletion decreases. Compared with the sub-STED method, which can only suppress the STED excitation-related background, psSTED has better background suppression performance, especially when relatively low STED power is used (Supporting Information, Figures S5 and S6). The background in the X-Z cross sections of STED images was much more severe than that in the X-Y cross sections, highlighting the critical need of background suppression in 3D STED.

High resolution STED imaging requires strong STED beam and high fluorescence labeling density, both of which contribute to background[20] (Figure 2a). To quantitatively address the background issue with varying STED intensities and labeling

DOI: 10.1021/acsphotonics.9b00537
ACS Photonics XXXX, XXX, XXX−XXX

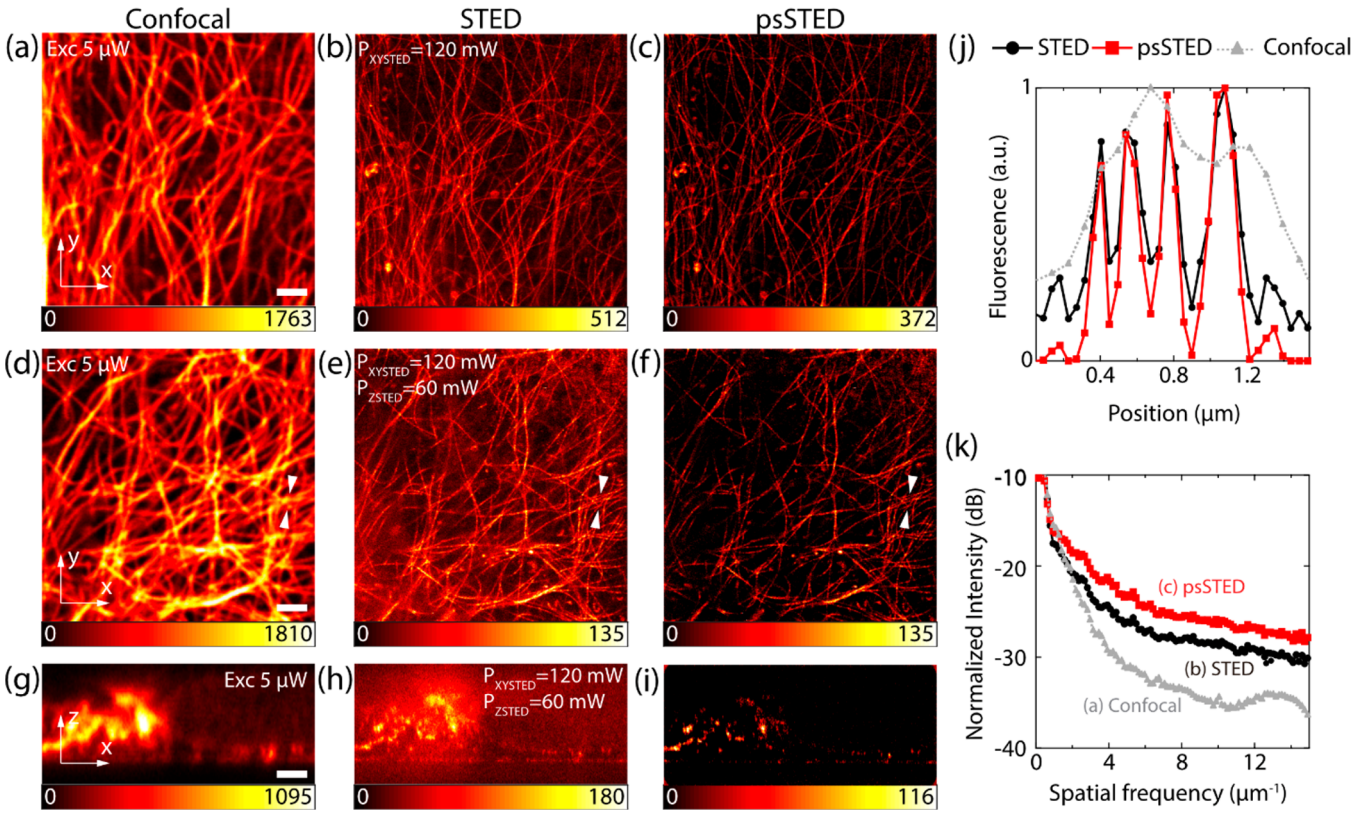

Figure 4. Images of SiR-tubulin-labeled microtubules in a 3T3 cell. Sampling steps: 45 nm in XY, 80 nm in Z. Pixel dwell time: 400 μs. Scale bar: 2 μm. (a) Confocal, (b) conventional 2D STED, and (c) 2D psSTED images; γ = 1.00. (d) Confocal, (e) conventional 3D STED, and (f) 3D psSTED images; γ = 1.00. (g) Confocal, (h) conventional 3D STED, and (i) 3D psSTED images in XZ plane; γ = 1.51. (j) The cross section of microtubule filaments (white arrow) in (d)−(f). (k) Spatial frequency analysis of the images in (g)−(i).

densities, we simulated a model system where fluorescent molecules are randomly located in 3D space with varying density and STED intensity, the example of which is shown in Figure 2b. In the simulated beads images it was clear that psSTED achieves much better SBR as compared to conventional STED. We employ peak signal-to-background ratio (PSBR) in X-Z cross sectional image of these molecules as a figure of merit[16] (see Methods for the definition of PSBR). As shown in Figure 2c, where STED power is fixed to 300 mW and the fluorescent molecule density is varied, higher molecule (or labeling) density significantly increases background and decreases PSBR in conventional 3D STED imaging. We assumed the power ratio 2:1 between XY-STED and Z-STED beams. However, by applying the psSTED method, PSBR increases by about 2 orders of magnitude. In Figure 2d, the molecule density is fixed to 10000 molecules/μm^3 and the STED power is varied. Because of the background problem, PSBR decreases as STED power increases. Applying psSTED attains the benefit of sharper PSF without the background effect, hence, the PSBR is significantly increased. Although psSTED achieves orders of magnitude improvement over conventional STED, the PSBR decreases as a function of molecule density.

psSTED Demonstration on Fluorescent Nanobeads. To demonstrate the effectiveness of psSTED experimentally, we used a 3D STED setup previously reported[9] with a modification, that is, mounting a half-wave plate (HWP) before the objective with a motor-driven rotational stage for switching the STED beam polarization between LCP and RCP (see Supporting Information, Figure S1 and Methods for details). Note that the same laser intensities and pixel dwell time were used for LCP and RCP recordings. After image-based drift correction and median filtering (see Methods) of the RCP image, we subtracted the RCP image from the regular STED image with a subtraction factor γ to obtain the background-subtracted psSTED image.

$$\text{psSTED} = \text{STED}_{\text{LCP}} - \gamma\,\text{STED}_{\text{RCP}}$$

γ corrects for photobleaching effect from sequential STED imaging and is experimentally determined from confocal images obtained before and after STED imaging (see Methods).

For the psSTED demonstration, we used single-layer fluorescent nanobeads mounted on a coverslip (20 nm crimson beads, ThermoFisher Scientific; Figure 3). The fluorescence lifetime of the crimson beads is 3.8 ns.[21] The background profile is affected by the density and the distribution of nearby fluorophores, excitation laser intensity, and by the STED laser wavelength and intensity (Supporting Information, Figures S5 and S6). Hence, we performed two sets of experiments, one with high STED power of 220 mW for XY-STED and 100 mW for Z-STED (Figure 3(a)-(d)) and the other with low STED power of 40 mW for XY-STED and 20 mW for Z-STED (Figure 3e−h). The lateral and axial full-width at half-maximum (fwhm) of individual nanobeads was 49.6 ± 10.0 nm and 145.2 ± 25.0 nm, respectively, with high STED power and was 98.1 ± 16.2 nm and 273.4 ± 40.3 nm with low STED power.

To quantitatively evaluate the background suppression performance, we calculated the signal to background ratio (SBR; see Methods) of each image. Here, SBR is defined as the ratio of on-fluorescence signal maxima to off-fluorescence averaged background. psSTED achieved a >10-fold improvement in SBR compared to regular STED [high STED power:

DOI: 10.1021/acsphotonics.9b00537
ACS Photonics XXXX, XXX, XXX−XXX

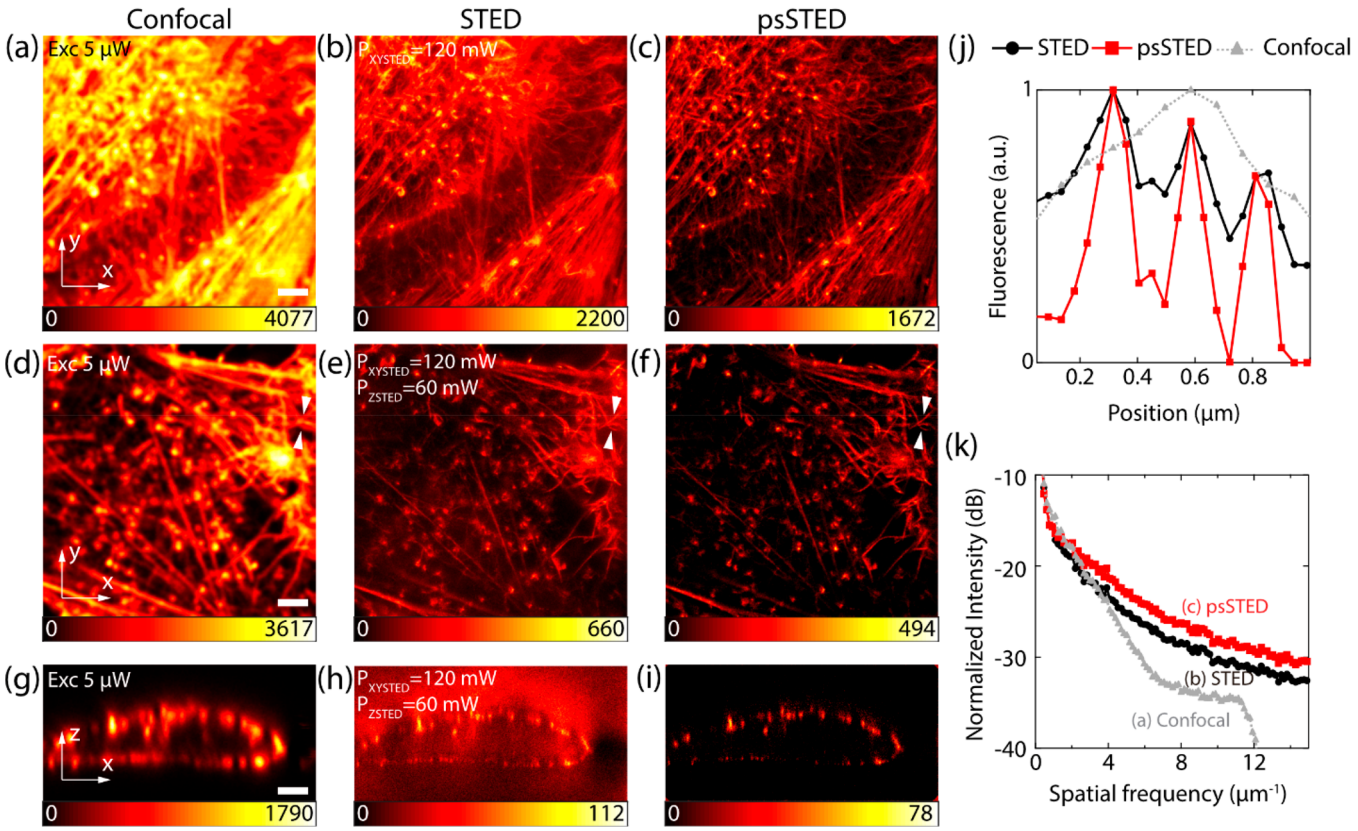

Figure 5. Images of a SiR-actin labeled actin structures in LN229 cell. Sampling steps: 45 nm in XY, 45 nm in Z. Pixel dwell time: 400 μs. Scale bar: 2 μm. (a) Confocal, (b) conventional 2D STED, and (c) 2D psSTED images; γ = 1.21. (d) Confocal, (e) conventional 3D STED, and (f) 3D psSTED images, where both XY STED and Z STED beams were applied; γ = 1.46. (g) Confocal, (h) conventional 3D STED, and (i) 3D psSTED images in XZ plane; γ = 2.25 (j) The cross section of actin filaments (white arrow) in (d)−(f). (k) Spatial frequency analysis of the images in (g)−(i).

SBR = 179 for psSTED (Figure 3d vs 17.1 for STED (Figure 3b); low STED power: SBR = 199 for psSTED (Figure 3h) vs 17.3 for STED (Figure 3f)]. In comparison, the sub-STED method did not show improvement compared to regular STED [SBR = 17.8 for high STED power (Figure 3c) and SBR = 17.3 for low STED power (Figure 3g)]. This is because the major background source here is not the direct excitation from STED laser (crimson beads have small excitation cross section at the STED wavelength), which sub-STED is designed to suppress. Main source of background noise in this particular case is rather the incomplete depletion, which sub-STED is not good at tackling. These results show that psSTED can achieve background suppression superior to sub-STED in both power regimes. The cross sections of beads along longitudinal axis (Figure 3i,j) again confirm that psSTED subtracts the background more effectively than sub-STED.

psSTED Demonstration on Biological Samples. Next, we conducted a series of psSTED experiments on biological samples. SiR-tubulin[22] labeled microtubules in mouse embryo fibroblast cells (3T3) were imaged with both 2D STED (Figure 4a−c) and 3D STED (Figure 4d−i), and comparison was made between confocal, STED, and psSTED. psSTED counteracts the background well and reveals the super-resolved details that are otherwise obscured by the background, as indicated by dramatically improved SBR: from 10.2 (Figure 3e) to 66.4 (Figure 4f). In X-Z sections, Figure 4g−i, the improvement of SBR is more dramatic: from 2.16 (Figure 4h) to 125 (Figure 4i). SBR of an image is defined in Methods. The fwhm of the microtubules in the psSTED images was 53.9 ± 6.8 nm and 174.6 ± 41.1 nm along the lateral and axial directions, respectively. Note that subtraction factor γ is employed to correct for photobleaching effect from sequential STED imaging (see Methods). The background suppression capability of psSTED was further visualized by plotting a line profile across the image (Figure 4j; white arrow in Figure 4d−f). The imaging contrast was enhanced and the adjacent microtubules were more clearly distinguished in psSTED. We also compared the spatial frequency component distribution of the images in Figure 4 expressed in the polar coordinate (Supporting Information, Figure S7). Spatial frequency analysis data quantitatively show that the low spatial frequency components are suppressed and the high spatial frequency components, which were before hidden in background noise, are relatively strengthened in psSTED compared to STED and confocal images (Figure 4k and Supporting Information, Figure S7).

We next imaged actin filament bundles in human glioblastoma cells (LN229) labeled with SiR-actin[22] using both 2D STED (Figure 5a−c) and 3D STED (Figure 5d−i). Again, we achieved effective background suppression in psSTED compared to STED in all conditions, as evidenced by the largely increased SBR in all images, for example, from 2.91 (Figure 5h) to 31.3 (Figure 5i). The fwhm of the actin filament bundles was 90.7 ± 19.4 nm and 190.6 ± 60.7 nm along the lateral (Figure 5f) and axial (Figure 5i) directions, respectively. The line profile plot (Figure 5j), indicated with white arrows in Figure 5d−f, clearly shows an improved contrast. In the spatial frequency domain analysis, psSTED suppresses low spatial frequency components while preserving high spatial frequency components (Figure 5k

DOI: 10.1021/acsphotonics.9b00537
ACS Photonics XXXX, XXX, XXX−XXX

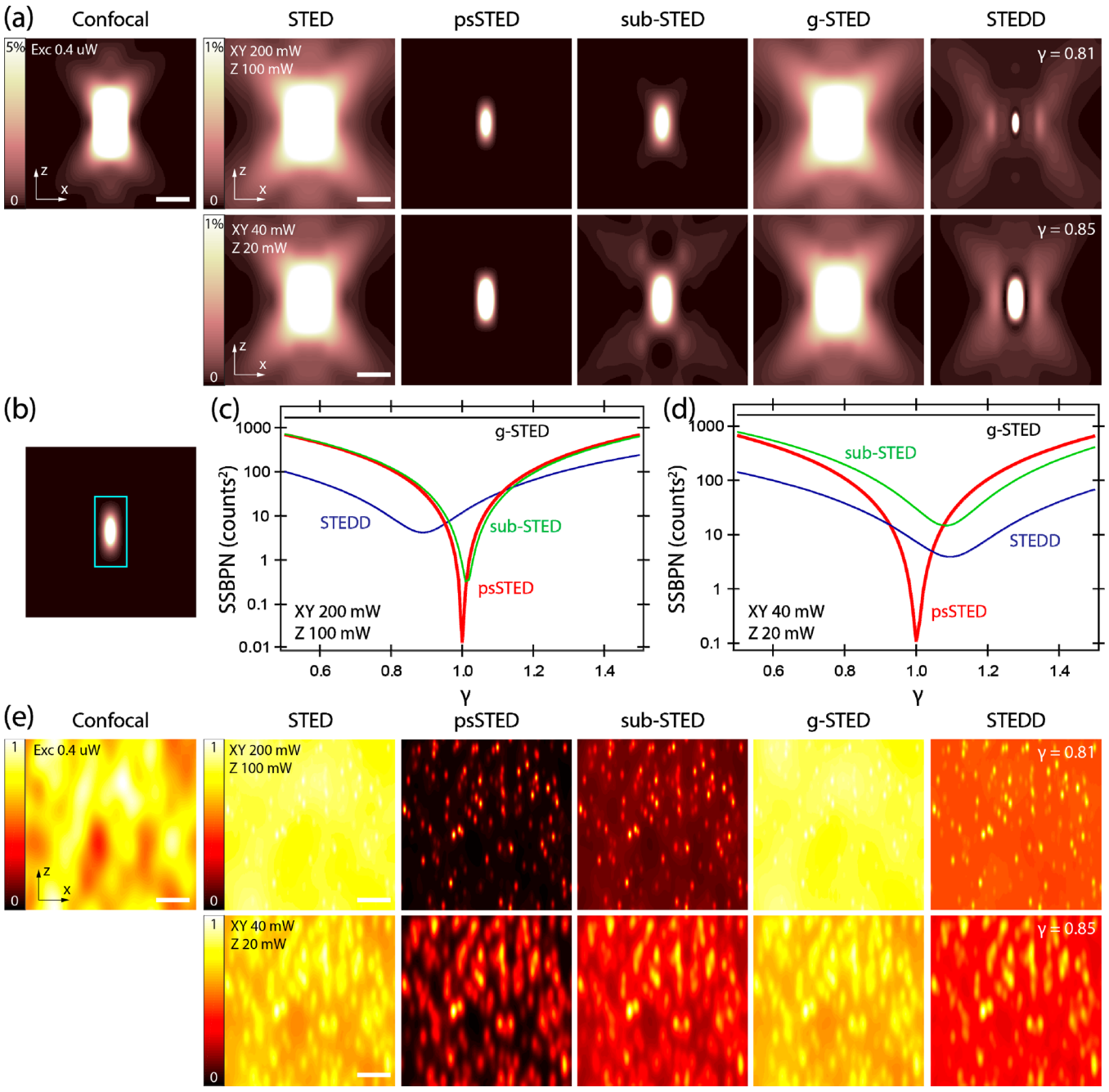

Figure 6. Comparison of psSTED performance with other background suppression methods: STEDD, sub-STED, and g-STED. (a) Comparison of effective point spread function (PSF). The fluorescence intensity is calculated by assuming a point fluorophore, quantum yield of excitation = 0.65, pulse period = 12.5 ns, dwelling time = 400 μs, SPCM efficiency = 0.9. The number in the color map represents the percent intensity normalized to the maximum intensity across the PSF. The intensity higher than the highest value in the color map appears as white. Scale bar: 500 nm. (b) The sum of squared background photon number (SSBPN) is calculated from the images from (a) except for the center area to exclude signal fluorescence photons. The area excluded in the SSBPN calculation is shown in cyan color. SSBPN as a function of subtraction factor γ at high STED power (c) and low STED power (d). (e) Comparison of simulated fluorescent beads. Simulations of 5000 fluorescent beads are randomly scattered in a 2.56 × 2.56 × 2.56 μm space. The color map is normalized to the maximum intensity of each image. γ for STEDD is chosen to achieve minimum background while maintaining non-negative effective PSF. Scale bar: 500 nm.

and Supporting Information, Figure S8). Imaging with two different mammalian cells and proteins of interest, it demonstrates that psSTED exhibits significantly improved SBR in the images of biological samples.

Comparison to Other Background Subtraction Methods. We next compared the background subtraction performance of psSTED with that of previously reported sub-STED,[11,12] g-STED,[15] and STEDD[13,14] by simulating the spatial profile of detected fluorescence of a single fluorophore (Figure 6a). See Methods and Supporting Information for simulation details and parameters. sub-STED can only partially suppress the low-resolution background, mainly coming from the STED beam excitation, whereas the remaining background due to incomplete depletion is considerable, especially when low STED power is used. The time-gated g-STED approach can reduce the low-resolution background by selectively rejecting the early

DOI: 10.1021/acsphotonics.9b00537
ACS Photonics XXXX, XXX, XXX−XXX

Table 1. PSPN, BPN, and PSBR of Images of Simulated Beads in Figure 6e

		STED	psSTED	sub-STED	g-STED	STEDD
high STED power (300 mW)	PSPN	1060	787	840	798	308
	BPN	3388	8	85	2673	266
	PSBR	0.313	98.4	9.88	0.300	1.16
low STED power (60 mW)	PSPN	5128	1945	2552	3950	798
	BPN	2892	22	476	2233	309
	PSBR	1.77	88.4	5.36	1.77	2.58

photons that suffer from incomplete depletion. However, it appears to be ineffective at suppressing the background at the periphery. STEDD appears to sharpen the central area of the PSF, while the peripheral background persists. In contrast, psSTED exhibits the best background subtraction performance no matter which STED beam intensity regime is used, thanks to its ability to estimate accurately the low-resolution background in the RCP mode (Figures 6 and S3). As a figure of merit for quantifying how well the background is subtracted, we defined the sum of squared background photon number (SSBPN): SSBPN = Σ(photon number)^2 outside of the rectangle where fluorescence signal is detected (Figure 6b).

The size of the rectangle is reasonably chosen to be 480 nm (in X) × 1056 nm (in Z) and is centered around the object imaged (Figure 6b). In an ideal background-subtracted image, SSBPN must be zero. Hence, the smaller the SSBPN is, the better the background subtraction. Clearly, in both high and low STED intensity regimes, the unambiguous choice of $\gamma = 1$ in psSTED (photobleaching was not included in the simulation) offers the best background subtraction compared to all three techniques: STEDD, sub-STED, and g-STED (Figure 6c,d). In the case of STEDD and sub-STED, an additional step to determine subtraction factor γ is required. We also compared psSTED performance with confocal subtraction, that is, subtracting a confocal image from a STED image to achieve better SBR, and confirmed that psSTED is superior to confocal subtraction method (Figure S9).

Next, we simulated randomly located fluorescent beads in 3D space to compare the background subtraction techniques (Figure 6e). At both high and low STED power regimes, psSTED subtracted the background much better than the other methods. Peak signal photon number (PSPN), background photon number (BPN), and PSBR values of images are shown in Table 1.[13] See Methods for the definition of PSPN, BPN, and PSBR. psSTED achieves much higher PSBR compared to other methods. Note that psSTED images are at least twice brighter than the STEDD images. Hence, although psSTED requires acquiring data twice (with LCP and RCP), the STEDD method must also acquire data for at least twice longer to achieve the same brightness as psSTED. Qualitatively and quantitatively, psSTED outperforms the previously proposed methods for background subtraction while providing ease and simplicity of the implementation. We also compared different background subtraction methods at different levels of excitation power to emphasize the effect of excitation power on background (Supporting Information, Figure S10). Again, psSTED is shown to outperform the others.

DISCUSSION

Because the STED effect is nonlinear in STED beam intensity, the spatial profile of the background can be a complex function of multiple variables, such as the intensity and wavelength of STED and excitation lasers, the density and the distribution of the nearby fluorophores, STED and excitation pulse widths, and the property of the label itself. From the simulations and experimental results, we demonstrated that psSTED suppresses the background in different imaging conditions, where different background sources dominate. In comparison to other background suppression methods, psSTED is much simpler, easier to implement, and more effective. An additional half-wave plate is essentially the only necessary component for psSTED. While the performances of other methods heavily depend on different parameters, such as STED intensity and wavelength, excitation intensity and wavelength, labeling density, and subtraction factor, psSTED outperforms the other methods in all conditions. Although psSTED was demonstrated with a motorized rotation stage in this work, polarization switching can also be achieved pixel-by-pixel by using an electro-optic modulator (EOM) if fast switching is desired for high speed live-cell imaging[23] or for fluorescence correlation spectroscopy (FCS) applications.[24] Additionally, such fast polarization switching will make it unnecessary to measure the subtraction factor (γ). More involved devices such as complex timing circuitry or a time-correlated single photon counting (TCSPC) module is not needed in psSTED compared with other background suppression methods.[13−15] Furthermore, it is worth mentioning that psSTED method can be applicable to both continuous-wave (CW) STED and pulsed STED unlike STEDD.

METHODS

Peak Signal-to-Background Ratio (PSBR) Calculation. From the maximum photon number (Max) and minimum photon number (Min) of the images, we calculated the peak signal photon number (PSPN) and background photon number (BPN): PSPN = Max − Min, BPN = Min. Then the peak signal-to-background ratio (PSBR) is calculated as PSBR = PSPN/BPN[16]

Bead Sample Preparation. A coverslip and a glass slide were washed with water and ethanol and then dried with dry air. They were then incubated with poly-L-lysine for 5 min to facilitate the attachment of fluorescent beads to the glass surface, followed by thorough washing with water and drying. Double sided tape is applied in between the coverslip and glass slide to make a chamber for fluorescent beads. Crimson beads (20 nm, 2% solid, ThermoFisher Scientific) were diluted 10000 times into 1 M Tris HCl pH 7.5 solution and were flowed in the chamber. The chamber was sealed with 5 min epoxy glue and incubated for at least 1 h in the dark.

Cell Sample Preparation. The mouse embryo fibroblast cells (3T3, ATCC) were cultured at 37 °C and 5% CO_2 in Dulbecco's modified Eagle's medium with 10% fetal bovine serum and 1× Gibco Antibiotic-Antimycotic (Thermo Fisher Scientific). Eight-well Lab-Tek II chambered cover-glass (Thermo Fischer Scientific) or glass bottom dish (In Vitro Scientific) were coated with fibronectin (Sigma) for 1 h before cells are seeded. After 24−48 h culturing (~80% confluency),

DOI: 10.1021/acsphotonics.9b00537
ACS Photonics XXXX, XXX, XXX−XXX

the cells were fixed with 10 mM ethylene glycol bis(succinimidyl succinate) (EGS, Thermo Fisher Scientific) for 10 min and washed with 1× phosphate buffered saline (PBS) three times. The cells were then treated with 0.2% Triton X-100 for permeabilization, washed with 1× PBS three times, and incubated with 500 nM SiR-tubulin (Cytoskeleton, Inc.) for 30 min. After gentle washing 3×, the cells were imaged in 1× PBS.

The human glioblastoma cells (LN229, ATCC) were cultured at 37 °C and 5% CO_2 in Dulbecco's modified Eagle's medium with 10% fetal bovine serum and antibiotics (100 unit mL^{-1} penicillin and 100 μg mL^{-1} streptomycin). Eight-well Lab-Tek II chambered coverglass (Thermo Fischer Scientific) or glass bottom dish (In Vitro Scientific) were coated with fibronectin (Sigma) for 1 h before cells are seeded. After 24−48 h culturing (~80% confluency), the cells were fixed with 4% paraformaldehyde (Electron Microscopy Sciences) for 10 min and then washed with 1× phosphate buffered saline (PBS) three times. The cells were then treated with 0.5% Triton X-100 (optional), washed with 1× PBS three times, and incubated with 400 nM SiR-actin (Cytoskeleton, Inc.) for 30 min. After gentle washing 3×, the cells were imaged in 1× PBS.

Home-Built STED Microscope. Our microscope employs a mode-locked Ti:sapphire femtosecond laser (MaiTai HP, Spectra Physics), which generates a train of <100 fs pulses at 80 MHz repetition rate. The laser is split into two beam paths for STED and excitation beams using HWP and PBS. STED laser pulse is stretched by two 15 cm long glass rods (N-SF57, Casix) and a 100 m long polarization maintaining single-mode fiber (PMJ-A3AHPC,3S-633-4/125-3-100-1-SP, OZ optics) to the final pulse width of approximately 300 ps. The two glass rods are mounted on a translation stage (PRL-12, Newport) so that the delay between the STED pulse and the excitation pulse can be optimized. In the excitation beam path, the supercontinuum light was generated by the 12 cm long photonic crystal fiber (FemtoWhite 800, NKT photonics) and was spectrally filtered using a short pass filter (FF01-680/SP, Semrock). A 15 cm long glass rod (N-SF57, Casix) stretches the excitation laser pulse to <100 ps. The supercontinuum was then triply filtered by an acousto-optic tunable filter (AOTFnC-400.650, AA Optoelectronic) and coupled to a single-mode fiber (P5−488PM-FC-2, Thorlabs) to be used as an excitation beam. The triple-pass acousto-optic tunable filter allows the excitation beam to be wavelength selected or turned on/off with 1 μs response time and 1−2 nm bandwidth.

The fiber-delivered STED laser is collimated, spectrally filtered, and split by a HWP and a PBS with a variable splitting ratio. Each beam passed through a phase plate imprinted with a $0-2\pi$ vortex (VPP-1, RPC photonics) or $0-\pi$ binary circle to generate a XY- or Z-STED beam, respectively. The two STED beams were recombined at a 5 mm thick dichroic beam splitter (z740sprdc, Chroma) and left circularly polarized using an achromatic quarter-wave plate and a half-wave plate (RAC 4.4.15 and RAC 4.2.15, B. Halle Nachfl). The excitation beam was reflected by a 30:70 (R:T) beam splitter (BS019, Thorlabs). The fluorescence signal was collected by an oil immersion objective (1.4 NA HCX PL APO 100x, Leica) and spectrally filtered by BLP01-635R-25 (Semrock) and ET670/40 m (Chroma). Then, the fluorescence signal was imaged onto multimode fibers with a core diameter of 62.5 μm (M31L01, Thorlabs) and detected by a single-photon counting module (SPCM-AQR-14-FC, PerkinElmer). The sample was scanned by a 3-axis piezo translational stage (MAX311D, Thorlabs); Imspector software was used for data collection.

Polarization Switching. Polarization switching is achieved by rotating the HWP by $\pi/4$ using a motorized rotation stage (PRM1Z8). Rotation of HWP flips the vertically (horizontally) polarized light into horizontally (vertically) polarized light, which is, after the quarter-wave plate, effectively switching LCP(RCP) to RCP(LCP).

Drift Correction. To correct the stage drift in between the regular STED image and background noise image, an image based drift correction was employed. The cross-correlation of the two images is calculated and the peak position of the cross-correlation was identified. The background noise image is shifted by the peak position accordingly.

Median Filter. Our noise suppression scheme subtracts the background noise image from the regular STED image. Upon subtraction, the variance of the output becomes $\sigma^2_{A-B} = \sigma^2_A + \sigma^2_B$. If the random salt and pepper noise exists in both of the images, subtraction can increase the amplitude of the random noise. To avoid this, we applied a median filter of (15,15) pixels on the background image.

SBR Calculation. SBR can be calculated by estimating background by averaging the signal from the off-fluorescence region and dividing it from on-fluorescence signal maxima, $\mathrm{SBR} = \frac{I_{on}}{I_{off}}$.

Photobleaching Correction. In case substantial photobleaching occurs during subsequent STED imaging, the background image with RCP can be dimmer, leading to an underestimation of the background noise. A subtraction factor γ is estimated by dividing the total intensity of the confocal image of the same area before (I_{BS}) and after (I_{AS}) regular (LCP) STED imaging: $\gamma = I_{BS}/I_{AS}$. Finally, the photobleaching artifact is corrected by $\mathrm{psSTED} = \mathrm{STED_{LCP}} - \gamma\mathrm{STED_{RCP}}$. Typically, γ ranged from 1.0 to 2.25.

Theoretical Simulation Parameters. In the case of psSTED and sub-STED, there is no time-gating, that is, all photons in the time domain are collected, although psSTED can readily be combined with time-gating for a sharper PSF. In the case of g-STED, we set the detection delay to 600 ps after the peak of STED pulse.[15] In the case of STEDD, we chose a second Gaussian STED power to be 10% of the first pulse with a 2 ns delay with respect to the first pulse, as suggested in ref 14. We determined the subtraction factor γ such that the effective PSF (Figure 6a) does not include negative values to avoid oversubtraction. The detection time windows for STED1 and STED2 are from 0 to 2 ns and from 2.2 to 5.3 ns after the peak of first STED pulse, respectively.[13,14] For psSTED, γ = 1 was chosen unambiguously. See Supporting Information for detailed simulation parameters.

Spatial Frequency Analysis. To analyze confocal, STED, and psSTED images more quantitatively, a 2D Fourier transform is performed to transfer the image to the 2D spatial frequency space. Then, the 2D Fourier transformed image is coordinate-transformed into polar coordinate (θ,r). The intensity as a function of spatial frequency can be calculated by integrating it over angular (θ) coordinate, and normalizing it to make the sum of all intensities to 1.

DOI: 10.1021/acsphotonics.9b00537
ACS Photonics XXXX, XXX, XXX−XXX

■ ASSOCIATED CONTENT

Supporting Information

The Supporting Information is available free of charge on the ACS Publications website at DOI: 10.1021/acsphotonics.9b00537.

Details of experimental schematics, PSF changes upon polarization switching, simulation of PSFs, energy level diagram, simulation of fluorescent beads, experimental results of fluorescent beads, spatial frequency analysis, additional comparisons to other background subtraction methods, pulse delay optimization, background noise analysis, and a detailed calculation of the results (PDF)

■ AUTHOR INFORMATION

Corresponding Author

*E-mail: tjha@jhu.edu.

ORCID

Jong-Chan Lee: 0000-0003-3073-4657
Ye Ma: 0000-0002-0402-5964
Kyu Young Han: 0000-0002-1448-3125
Taekjip Ha: 0000-0003-2195-6258

Notes

The authors declare the following competing financial interest(s): The authors are applying for a patent of the technique demonstrated in the manuscript.

■ ACKNOWLEDGMENTS

The work was funded by a grant from the National Institutes of Health (GM122569) and National Science Foundation (PHY-1430124 Physics Frontiers Center Program). This work was also supported by the National Research Foundation of Korea (NRF-2018R1C1B5045902, NRF-2019K2A9A2A12000363, NRF-2019R1F1A1057948) and DGIST HRHR program of the Ministry of Science, ICT and Future Planning. K.Y.H. acknowledges support from National Science Foundation (1805200).

■ REFERENCES

(1) Betzig, E.; Patterson, G. H.; Sougrat, R.; Lindwasser, O. W.; Olenych, S.; Bonifacino, J. S.; Davidson, M. W.; Lippincott-Schwartz, J.; Hess, H. F. Imaging Intracellular Fluorescent Proteins at Nanometer Resolution. *Science (Washington, DC, U. S.)* **2006**, *313* (5793), 1642−1645.

(2) Rust, M. J.; Bates, M.; Zhuang, X. Stochastic Optical Reconstruction Miscroscopy (STORM) Provides Sub-Diffraction-Limit Image Resolution. *Nat. Methods* **2006**, *3* (10), 793−795.

(3) Klar, T. A.; Hell, S. W. Subdiffraction Resolution in Far-Field Fluorescence Microscopy. *Opt. Lett.* **1999**, *24* (14), 954−956.

(4) Klar, T. A.; Engel, E.; Hell, S. W. Breaking Abbe's Diffraction Resolution Limit in Fluorescence Microscopy with Stimulated Emission Depletion Beams of Various Shapes. *Phys. Rev. E: Stat. Phys., Plasmas, Fluids, Relat. Interdiscip. Top.* **2001**, *64* (6), 066613.

(5) Rittweger, E.; Han, K. Y.; Irvine, S. E.; Eggeling, C.; Hell, S. W. STED Microscopy Reveals Crystal Colour Centres with Nanometric Resolution. *Nat. Photonics* **2009**, *3* (3), 144−147.

(6) Leutenegger, M.; Eggeling, C.; Hell, S. W. Analytical Description of STED Microscopy Performance. *Opt. Express* **2010**, *18* (25), 26417−26429.

(7) Hein, B.; Willig, K. I.; Hell, S. W. Stimulated Emission Depletion (STED) Nanoscopy of a Fluorescent Protein-Labeled Organelle inside a Living Cell. *Proc. Natl. Acad. Sci. U. S. A.* **2008**, *105* (38), 14271−14276.

(8) Osseforth, C.; Moffitt, J. R.; Schermelleh, L.; Michaelis, J. Simultaneous Dual-Color 3D STED Microscopy. *Opt. Express* **2014**, *22* (6), 7028.

(9) Han, K. Y.; Ha, T. Dual-Color Three-Dimensional STED Microscopy with a Single High-Repetition-Rate Laser. *Opt. Lett.* **2015**, *40* (11), 2653.

(10) Ma, Y.; Ha, T. Fight against Background Noise in Stimulated Emission Depletion Nanoscopy. *Phys. Biol.* **2019**, na.

(11) Hanne, J.; Falk, H. J.; Görlitz, F.; Hoyer, P.; Engelhardt, J.; Sahl, S. J.; Hell, S. W. STED Nanoscopy with Fluorescent Quantum Dots. *Nat. Commun.* **2015**, *6* (May), 7127.

(12) Vicidomini, G.; Moneron, G.; Eggeling, C.; Rittweger, E.; Hell, S. W. STED with Wavelengths Closer to the Emission Maximum. *Opt. Express* **2012**, *20* (5), 5225.

(13) Gao, P.; Ulrich Nienhaus, G. Precise Background Subtraction in Stimulated Emission Double Depletion Nanoscopy. *Opt. Lett.* **2017**, *42* (4), 831.

(14) Gao, P.; Prunsche, B.; Zhou, L.; Nienhaus, K.; Nienhaus, G. U. Background Suppression in Fluorescence Nanoscopy with Stimulated Emission Double Depletion. *Nat. Photonics* **2017**, *11* (3), 163−169.

(15) Vicidomini, G.; Moneron, G.; Han, K. Y.; Westphal, V.; Ta, H.; Reuss, M.; Engelhardt, J.; Eggeling, C.; Hell, S. W. Sharper Low-Power STED Nanoscopy by Time Gating. *Nat. Methods* **2011**, *8* (7), 571−573.

(16) Vicidomini, G.; Schönle, A.; Ta, H.; Han, K. Y.; Moneron, G.; Eggeling, C.; Hell, S. W. STED Nanoscopy with Time-Gated Detection: Theoretical and Experimental Aspects. *PLoS One* **2013**, *8* (1), e54421.

(17) Coto Hernàndez, I.; Peres, C.; Cella Zanacchi, F.; d'Amora, M.; Christodoulou, S.; Bianchini, P.; Diaspro, A.; Vicidomini, G. A New Filtering Technique for Removing Anti-Stokes Emission Background in Gated CW-STED Microscopy. *Journal of Biophotonics* **2014**, *7*, 376−380.

(18) Lanzanò, L.; Coto Hernández, I.; Castello, M.; Gratton, E.; Diaspro, A.; Vicidomini, G. Encoding and Decoding Spatio-Temporal Information for Super-Resolution Microscopy. *Nat. Commun.* **2015**, *6*, na.

(19) Hao, X.; Kuang, C.; Wang, T.; Liu, X. Effects of Polarization on the De-Excitation Dark Focal Spot in STED Microscopy. *J. Opt.* **2010**, *12* (11), 115707.

(20) Lau, L.; Lee, Y. L.; Sahl, S. J.; Stearns, T.; Moerner, W. E. STED Microscopy with Optimized Labeling Density Reveals 9-Fold Arrangement of a Centriole Protein. *Biophys. J.* **2012**, *102*, 2926.

(21) Willig, K. I.; Harke, B.; Medda, R.; Hell, S. W. STED Microscopy with Continuous Wave Beams. *Nat. Methods* **2007**, *4*, 915.

(22) Lukinavičius, G.; Umezawa, K.; Olivier, N.; Honigmann, A.; Yang, G.; Plass, T.; Mueller, V.; Reymond, L.; Corrêa, I. R., Jr; Luo, Z.-G.; et al. A Near-Infrared Fluorophore for Live-Cell Super-Resolution Microscopy of Cellular Proteins. *Nat. Chem.* **2013**, *5* (2), 132−139.

(23) Bottanelli, F.; Kromann, E. B.; Allgeyer, E. S.; Erdmann, R. S.; Wood Baguley, S.; Sirinakis, G.; Schepartz, A.; Baddeley, D.; Toomre, D. K.; Rothman, J. E.; Bewersdorf, J.; et al. Two-Colour Live-Cell Nanoscale Imaging of Intracellular Targets. *Nat. Commun.* **2016**, *7*, 10778.

(24) Lanzanò, L.; Scipioni, L.; Di Bona, M.; Bianchini, P.; Bizzarri, R.; Cardarelli, F.; Diaspro, A.; Vicidomini, G. Measurement of Nanoscale Three-Dimensional Diffusion in the Interior of Living Cells by STED-FCS. *Nat. Commun.* **2017**, *8* (1), 65.

DOI: 10.1021/acsphotonics.9b00537
ACS Photonics XXXX, XXX, XXX−XXX